Revisiting the Effect of Rib Roughness on the Performance of Solar Air Heater

Neeraj Kumar Nagayach[1], Kanishk Sharma[1], Yogesh Agrawal[2] and Anil Singh Yadav[3]*

[1]Department of Mechanical Engineering, JECRC University, Jaipur, Rajasthan, India-303905
[2]Department of Mechanical Engineering, SIRT, Bhopal, MP, India-462042
[3]Department of Mechanical Engineering, IES College of Technology, Bhopal, MP, India-462044

Abstract. The energy collected from various renewable resources, such as sunlight, geothermal warmth, wind, and water, is referred to as renewable power. The sun is the ultimate source of vitality. Solar radiation vitality can be utilized in many functions, such as heating buildings and dusty foliage crops, dying chicken, wood taste, and treating modern elements. All the energy patterns in nature asking them are the origin of the sun. The solar air heater (SAH) is very common along with commonly applied sun-oriented heating apparatus. Perhaps, SAH is utilized for a wide range of applications, from residential to commercial. Improving the SAH efficiency is done by applying rib elements on the bottom side of the roughness element ribs, grooves, fins, baffles, twisted tapes, deflectors, etc., and improved Thermo-hydraulic performance (THP). Various investigators have prepared several practices in their research work to obtain a greater transfer of thermal energy between these solar collector heaters by applying various rib elements to the absorbent surface. The objective of that study is obliged to describe and conclude tests on the impact of modest rib element height and face projection upon absorber plate along duct surface as artificial rib elements of different shapes on heat transfer along friction factor. The research on artificially roughened SAH ducting is thoroughly analyzed in this paper. The purpose of this paper is to summarize several studies on the thermal and hydraulic performance of synthetically roughened SAH ducting. For the analyzed range of parameters, it was discovered that the usage of arc-shaped-shaped rib geometry and metal grit ribs has the maximum THP parameters in comparison to often roughness geometry. For the tested range of parameters, the use of broken arc ribs has the highest Nu compared to the plain arc-shaped rib roughness. Arc configuration of roughness element exhibits fewer ranges pressure diminishes than the V form design because the produced secondary flow has a curved structure and is rougher.

Keywords: Ribs, Fluid flow, solar energy, Solar air heater, Heat transfer

1. Introduction

*Corresponding author: anilsinghyadav@gmail.com

Conventional energy sources have a limited supply of available resources. Therefore, more attention has to be paid to maximizing and applying renewable energy assets. The sun is the most powerful energy source. Such a gadget is a SAH, which transforms sun energy into heat energy. Figure 2 and presented types of flat
plat solar collector and flat plate SAH respectively. SAHs have various applications, including building heating, crop and fruit drying, chicken brooding, timber seasoning, and industrial product curing. It's worth noting that all energy on Earth has a solar origin. Solar energy has distinct advantages over other forms of energy due to its cleanliness and its ability to provide energy without any negative environmental impact [1]. Conventional SAHs can heat air more effectively by adding roughness to the underside of the absorber plate in many ways. The effectiveness of a SAH can be enhanced by a passive transfer of heat technique called artificial ribs. Incoming solar radiation is absorbed by SAH and converted into heat energy on the surface of the absorber plate. When air flows over an absorber plate, laminar and turbulent layers are formed over the plate's surface. Within these layers, close to the plate's surface, a laminar sub-layer is formed due to the presence of the observer, which slows down heat transfer to the flowing air and affects the thermal performance of the SAH. Artificially roughened absorber plates are the most suited solution to achieve a better heat transfer coefficient and solve this issue. As a result, the heat transfer coefficient was artificially increased to break up the laminar sub-layer and lower thermal resistance. In order to minimize friction loss, it is therefore preferable to induce a disturbance in the area immediately next to the surface of heat transfer, i.e., in the sub-layer of laminar alone [2].

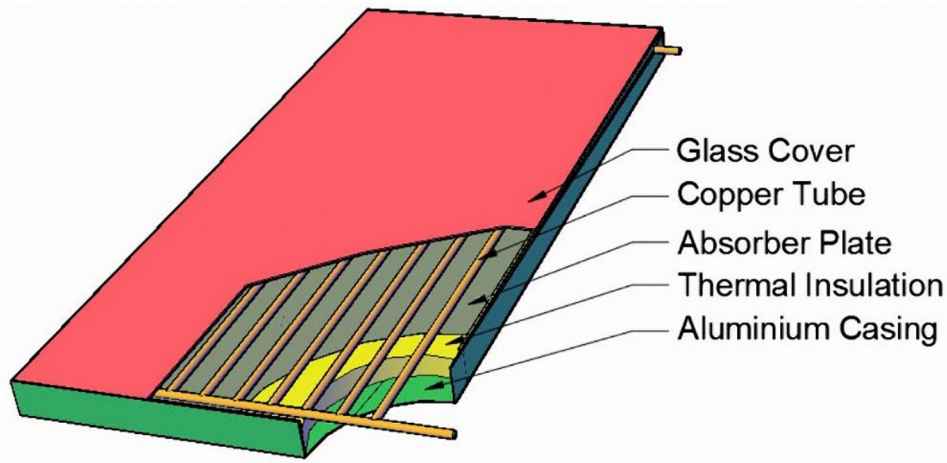

Figure 1. Flat plate solar collector [3]

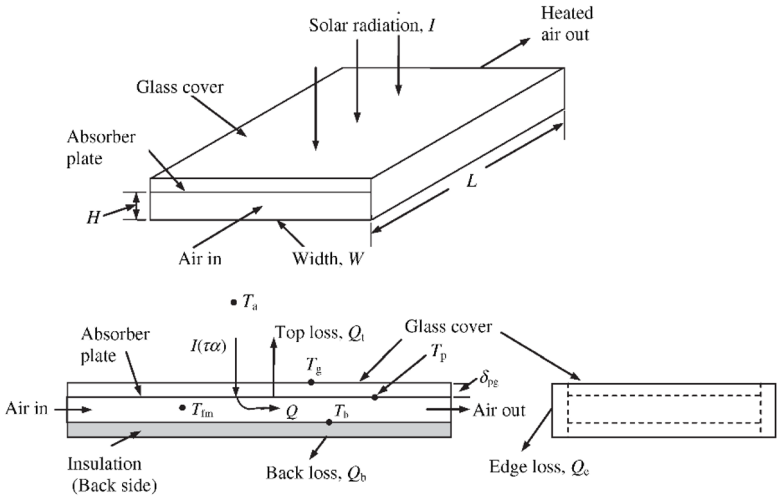

Figure 2. Flat plate SAH [2]

Artificial roughened SAHs are usually subjected to a lot of experimentation and time-consuming development. Due to the advent of computational fluid dynamics the design and optimization of these air heaters has been greatly simplified. The computational method is an efficient method of tackling the complicated problem of designing and optimizing of roughened SAHs that involves a wide range of complex and wide-ranging parameters. This technology has seen a significant uptick in adoption rates over the past few years in the design and optimization of SAHs. The results of these simulations show that the use of this tool is very effective in predicting the performance and behaviours of the air heater. In-depth evaluations on the SAH were presented in excellent review papers that took an experimental approach [4-7]. The performance of SAH have been thoroughly analysed in a number of excellent review studies that take a computational approach [8-11].

1.1 Artificial roughness fundamentals

A passive heat transfer augmentation technology called artificial roughness can improve the THP of a SAH. Artificial roughness has substantially improved forced convective heat transfer, which also requires turbulent flow at the heat-transferring surface. However, the energy to create such turbulence must come from the fan or blower, and a tremendous amount of power is required to drive air through the duct. It is preferred for the turbulence to only arise in the region that is extremely close to the heat-transfer surface in order to minimize power consumption. By keeping a low roughness element height with the duct size, this can be accomplished. It has been shown that a more W/H rectangular channel that is symmetrically heated and is designed after SAH Channel considerably enhances the heat transfer coefficient along least amount for pressure loss penalty by adding rib elements to the surface of heat transfer [12].

This review paper's goal is to provide an overview of the work done to improve SAH performance by using artificial roughness/turbulators in a variety of configurations. To determine the ideal rib configuration, a laboratory inspection of different rib element geometry is also provided. The viewers of that inspection who are involved in improving heat transfer will find it useful. The idea of artificial roughness and its accompanying effect is

covered in the subsection that follows. Also covered in detail is the performance of SAH with simulated roughness. Lau, McMillin and Han [13] examined the produced flow of air on a square duct along discrete turbulators in view of heat transfer coefficient (h) and friction factor (f). The e/Dh and p/e were both 0.0625 and 10, respectively. Re is 10,000 - 80,000. The outcomes reflected that mean Stanton number (St) in 90o unique rib instances was around 10-15% more compared to 90o roughness element of transverse form cases. Zhang, Gu and Han [14] investigated the effect of compound turbulators on SAH. The rib-groove roughened wall incurred a 6 times greater pressure drop penalty and increased heat transmission by 3.4 times, compared to the rib-roughened wall, which had similar rib height and rib spacing and increased heat transfer by 2.4 times. Karwa [15] investigated the effect of different shape ribs in SAH. Due to an increase in the Nu, this study demonstrated a significant improvement in ηth10–40% = over SAH with plain absorber panels (50-120 percent). Absorber face of SAH's channel, Bopche and Tandale [16] tested h and f of specially designed inverted U-shaped turbulators. Re of 3800-18000, e/Dh between 0.0186 and 0.03986, and p/e between 6.67 and 57.14 were covered by the trials. Throughout the entire trial, the flow on turbulators was targeted at an angle of 90o. In comparison to the plain channel, the turbulator-roughened duct increases Nu and f by 2.82 and 3.72 times, respectively. Correlations between the averaged Nu and f for the turbulator-roughened duct were obtained. When using the parameters W/H of 8, e/Dh of 0.0168–0.0338, p/e of 10, Re of 3000–15000, and α of 30–75o, Kumar, Bhagoria and Sarviya [17] evaluated THP of SAH along discrete W form ribs on the absorber face plate. Additionally, correlations for the Nu and f were computed using the range of values selected. They found that for e/Dh=0.0338 and α=60o, the friction factor is 2.75 and the increase in Nu is 2.16 in contrast to a plain SAH. In a test, Lanjewar, Bhagoria and Sarviya [18] looked at Nu along friction properties of a rectangular channel single broad fence that was roughened on the bottom by W-shaped ribs that were positioned perpendicular to the flow direction. The range of variables used was W/H of 8, p/e of 10, e/Dh of 0.018-0.03375, Re of 14000, and α of 30-75o. The greatest enhancement of Nu and f over a smooth channel for an α of 60o was found to be 2.36 and 2.01, respectively. Based on a turbulent flow via a SAH roughened duct, Yadav and Bhagoria [19] used CFD to model and simulate turbulent flows across SAH along square-cut form transverse roughness elements. Three different p and e values have been taken into consideration, with p/e = 14.29 being one of them. Re, varies between 3800 and 18,000. There is a range of 0.021 to 0.06 in e/Dh. According to the CFD predictions, e/Dh has a significant impact on the average Nu, average f, and THPP. For the range of parameters examined, a maximum value of the THPP of 1.8 has been discovered. Yadav and Bhagoria [20] conducted an evaluation of the application of CFD in the development of SAH. Outcomes of computations seem to show that for 2-D flow via conventional SAH, the RNG model yields the best results. Yadav and Bhagoria [21] explored 2-D incompressible Navier-Stokes flow through the purposefully roughened SAH pertinent Re ranges between 3800 and 18,000 in numerical research. Twelve unique equilateral triangular sectioned rib configurations (p/e of 7.14-35.71 and e/Dh of 0.021-0.042) have been employed as roughness elements. A numerical technique based on finite volumes is used. ANSYS FLUENT simulates the turbulent airflow through a synthetically roughened SAH. A SAH that has been purpose fully roughened is evaluated to determine the appropriate roughness element design. Lanjewar, Bhagoria and Agrawal [22] designed evolution for many rib geometries used to create artificial roughness. There are offered the connections between f and Nu discovered by different academics. It is proven that the performance evaluation for various double arc rib roughness orientations. Gawande, Dhoble, Zodpe and Chamoli [23] to simulate 20o angled ribs and analyse mathematical modelling and simulation methods for thermal performance optimization, a MATLAB approach was employed. Gawande, Dhoble, Zodpe and Chamoli [24] performed experimental and CFD studies using reverse L-shaped ribs with

Re of 3800–18000, e/Dh of 0.042, p/e of 7.14–17.86, and heat flow of 1000W/m2 have been used to evaluate the THP of a SAH. Using the RNG k-e turbulence model and the CFD code, ANSYS FLUENT, a 2D CFD simulation is carried out.

1.2 Enhancement of heat transfer through artificial rib elements in SAH

SAHs often use artificially rough surfaces to boost the heat transfer up to the laminar sub-layer. Adding ribs to the heated surface can further boost heat transfer by disturbing the viscous sub-layer and generating flow turbulence, separation, and reattachment, which can result in a higher heat transfer coefficient. The ribs are located exclusively on the heated wall, while the remaining all walls are flat and insulated. This setup is frequently observed in SAHs that feature absorber plates with artificial roughness. [25].

1.3 Performance analysis of SAH

In order to develop an effective system of this kind, it is necessary to conduct study on the thermal and hydraulic performance of a SAH:

1.3.1. Thermal performance: Using the Hottel–Whillier–Bliss equation, it is possible to compute the thermal performance of a SAH reported by

$$Q_{u=}A_C\ F_R\left[\ I(\tau\alpha)_e - U_L(T_i - T_a)\ \right] \quad (1)$$

or

$$q_{u=}\frac{Q_u}{A_c} = F_R\left[\ I(\tau\alpha)_e - U_L(T_i - T_a)\ \right] \quad (2)$$

Rate of valuable energy gain is given by

$$Q_{u=}\dot{m}\ c_p\ (T_o - T_i) = hA_c\left(T_{pm} - T_{am}\right) \quad (3)$$

Nusselt number (Nu) can be measured by

$$Nu = hl/k \quad (4)$$

In addition, the following equation can be used to express the thermal efficiency of a SAH

$$\eta_{th} = \frac{q_u}{I} = F_R\left[\ (\tau\alpha)_e - U_L(T_i - T_a)/I\ \right] \quad (5)$$

1.3.2. Hydraulic performance: According to the following equation, the pressure drop can be calculated as follows

$$\Delta P = \frac{2f\rho lv^2}{D} \quad (6)$$

where $f = 0.079\ R_e^{-0.25}$ (7)

1.3.3. Thermo-hydraulic Performance: Thermo-hydraulic performance (THP) can be calculated as follows

$$THP = \frac{{}^{Nu}/_{Nu_s}}{\left({}^{f}/_{f_s}\right)^{\frac{1}{3}}} \quad (8)$$

The design of a solar collector should be desirable and take into account both the THP features of SAH in view to incremented energy of heat and transfer to the flowing fluid with the least amount of fan energy consumption [26, 27].

1.4 Factors affecting the flow patterns of rib geometry

Roughness can be characterized by the following key dimensionless geometrical parameters:

1.4.1 Rib Height (e): It produces the following influence on the roughness element:

a. If e < δ There will be no roughness influence.
b. If e > δ There will be more roughness influence upon f as a contrast to Nu.
c. If e >δ There will be an enhancement in Nu and moderate f could be dealt.

1.4.2 Channel aspect ratio (W/H): That component is also highly important for finding THP. Table 1 shows the range of W/H for the enhanced rate of heat transfer:

Table 1 Ranges of W/H for an enhanced rate of heat transfer.

S. No.	Researchers	Roughness pattern	W/H Range
1.	Saini and Verma [28]	Dimple form roughness element	5
2.	Sahu and Bhagoria [29]	90o broken transverse rib	8
3.	Karmare and Tikekar [30]	Metal grit Roughness	10
4.	Saini and Saini [31]	Arc Shaped rib	12
5.	Aharwal, Gandhi and Saini [32]	Inclined roughness element in the uniform gap	5.87
6.	Kumar, Bhagoria and Sarviya [17]	Discrete W formed roughness element	8
7.	Varun, Saini and Singal [33]	Combination ribs	10
8.	Lanjewar, Bhagoria and Sarviya [34]	W-form rib element	8
9.	Singh, Chander and Saini [35]	Discrete roughness element in a v-down pattern	12
10.	Kumar, Saini and Saini [36]	Discrete V roughness element in multiple forms	12
11.	Yadav and Bhagoria [37]	Roughness element in circular protrusions in an angle arc pattern	11
12.	Bharadwaj, Kaushal and Goel [38]	Roughness element in inclined uniform manner	1.15
14.	Singh, Varun and Siddhartha [39]	Multiple arc shape	11
15.	Kumar, Kumar, Chauhan and Sethi [40]	Broken Multiple V-type baffles	10
16.	Deo, Chander and Saini [41]	Multiple V-down ribs	12
17.	Maithani and Saini [42]	V-ribs with Symmetrical gaps	10
18.	Kumar, Prajapati and Samir [43]	S Shaped rib	12

1.4.3 Channel height (h): SAH has more efficiency with lower channel height. The air velocity is increased by reducing channel height. The depth of SAH can be decreased to increase SAH efficiency.

1.4.4 Relative roughness pitch (p/e): It is the proportion of the height of the rib to the space between two adjacent ribs. Table 2 displays the maximal amount of transfer of heat for p/e.

1.4.5 Relative roughness height (e/Dh). It is defined as the ratio of the roughness element height to the equivalent air passage diameter. Nu and f both rise as e/Dh does. Table 2 displays the e/Dh value for maximal heat transfer rate.

1.4.6 Arc Angle (α). Through relation to the direction of air movement in the duct, this is how inclined the ribs are. By angling the rib with regard to the flow, counter-rotating secondary flow is generated along the length, which changes the h length-wise. Table 2 displayed α for the highest rate of heat transfer.

1.4.7 The shape of the roughness element. Ribs might be transverse or inclined, continuous or broken, with or without gaps, V-shaped, or they can be three-dimensional isolated elements. Additionally, the roughness elements may have intricate rib grooves, dimples, or wired arcs. The most common shape for ribs is square, although THP has also been studied with circular, semi-circular, and chamfered designs.

Table 2: Researchers, roughness pattern, Reynolds number and optimum performance parameter values of roughness elements.

S. No.	Researchers	Roughness pattern	Optimum performance parameter range of roughness elements		
			p/e range	e/Dh range	α range
1.	Prasad and Saini [44]	Transverse ribs	10	0.033	-
2.	Gupta, Solanki and Saini [45]	Roughness element in an inclined uniform manner	10	0.023	70o
3.	Karwa, Solanki and Saini [46]	Chamfered roughness element	7	0.044	-
4.	Ebrahim Momin, Saini and Solanki [47]	Roughness element in V pattern	10	0.033	60o
5.	Bhagoria, Saini and Solanki [48]	Roughness element in wedge manner	7.5	0.034	-
6.	Karwa [15]	Roughness element in combined transverse, inclined, v-up and down manner	10	-	60o
7.	Sahu and Bhagoria [29]	90o broken transverse rib	13	0.043	-
8.	Jaurker, Saini and Gandhi [49]	Roughness element in a grooved manner	6	0.037	-
9.	Karmare and Tikekar [30]	Metal grit roughness element	17.5	0.045	-
10.	Layek, Saini and Solanki [50]	Roughness element in the chamfered form	6	0.041	-
11.	Saini and Saini [31]	Arc-shaped roughness element	10	0.043	-
12.	Aharwal, Gandhi and Saini [32]	Roughness element in an inclined manner with a uniform gap	10	0.038	60o

13.	Saini and Verma [28]	Dimple form roughness element	10	-	-
14.	Kumar, Bhagoria and Sarviya [17]	Roughness element in discrete w manner	10	0.039	60o
15.	Varun, Saini and Singal [33]	Combination ribs	8	0.031	-
16.	Hans, Saini and Saini [51]	Roughness element in a multi v form	10	0.044	60o
17.	Lanjewar, Bhagoria and Sarviya [34]	W form roughness element	10	0.036	60o
18.	Singh, Chander and Saini [35]	Roughness element in the discrete v-down manner	10	0.044	60o
19.	Sethi, Varun and Thakur [52]	Roughness elements in a dimple arc form	8	0.037	-
20.	Kumar, Saini and Saini [36]	Roughness element in multi v-manner with the gap	12	0.044	60o
21.	Yadav and Bhagoria [37]	Circular protrusions in an angle arc form	12	0.03	60o
22.	Bharadwaj, Kaushal and Goel [38]	Roughness element in an inclined uniform manner	12	0.043	60o
23.	Singh, Varun and Siddhartha [39]	Multiple arc shape	8	0.045	60o
24.	Pandey, Bajpai and Varun [53]	Multiple arcs with gaps	8	0.044	60o
25.	Gawande, Dhoble, Zodpe and Chamoli [23]	200 square Section	7.14	0.0014	20o
26.	Gawande, Dhoble, Zodpe and Chamoli [24]	Reverse L-Shaped ribs	7.14	0.042	-
27.	Deo, Chander and Saini [41]	Multiple V-down ribs	10	0.045	-
28.	Maithani and Saini [42]	V-ribs with Symmetrical gaps	10	0.043	60o
29.	Kumar, Prajapati and Samir [43]	S Shaped rib	8	0.044	60o
30.	Sharma and Kalamkar [54]	Roughness element in combined truncated and thin continuous transverse wire form	10	0.055	90o
31.	Prakash and Saini [55]	Roughness element in combined spherical protrusion along with inclined protrusion	25	0.04	60o
32.	Singh Patel and Lanjewar [56]	V-shaped Ribs	10	0.043	60o
33.	Alam, Kumar and Balam [57]	Conical protrusion	10	0.0289	-
34.	Agrawal and Bhagoria [58]	Discrete double arc reverse pattern	8.33	0.027	60o

2. Various forms of roughness geometries used upon conventional SAHs

2.1 Transverse continuous rib

With a tiny diameter protrusion wire on the absorber plate, Prasad and Saini [44] experimentally examined the friction factor and heat transfer coefficient of the fully developed turbulent flow in a SAH duct. The kind and direction of the geometry are presented in Figure 3. The comparison revealed that the friction factor mean deviation was 6.3 percent and Nu mean deviation was 10.7 percent. The greatest improvements in heat transfer coefficient and friction factor exceeded those of a smooth duct by 2.38 and 4.25 times, respectively.

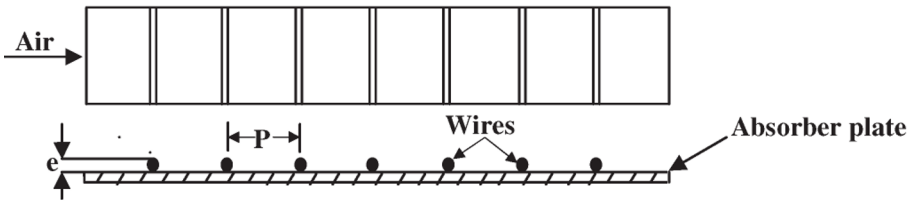

Figure 3 Transverse small diameter wire [44]

2.2 Roughness element in transverse broken form

By placing 90o discrete transverse roughness upon an absorber plate, Sahu and Bhagoria [29] reported the impact of SAH on h and ηth. Presented in Figure 4. With p ranges between 10 and 30 mm, e is 1.5 mm, W/H is 8, and Re is 3000–12000, the roughness geometry. Additionally, it was said that the maximum ηth and h values achieved were 1.23 to 1.42 more than and 83.5 % higher than those of a plain channel, respectively.

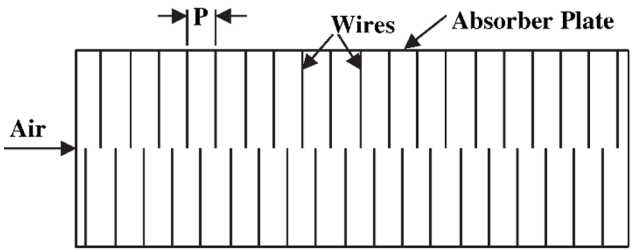

Figure 4 Transverse broken ribs [29]

In an experimental study, Varun, Saini and Singal [33] discovered that the SAH had thermal perforation with a roughness element combined type inclined and transverse roughness element, along Re =2000–14000, p/e = 3–8, and e/Dh = 0.030. The value for p/e at 8 was found to produce the best thermal performance.

2.3 Transverse inclined ribs

According to Kumar, Mittal, Thakur and Kumar [59], the experimental inspection was conducted to improve the h of a SAH that has an air duct that has been artificially roughened with 60o discrete inclined ribs. With such a roughness element, h has been significantly improved. Figure 5 depicts the geometry that was under investigation.

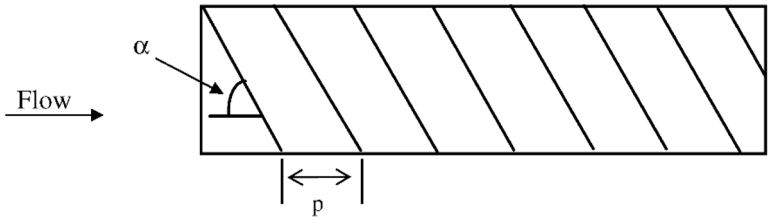

Figure 5 Transverse inclined continuous rib [59]

An equilateral triangle SAH ducts Nu and f properties were examined experimentally by Bharadwaj, Kaushal and Goel [38] employing roughness element uniform in inclined shaped upon absorber face. Re of 5600 - 28000, e/Dh of 0.021 -0.043, p/e of 8 - 16, W/H of 1.15, and α =30-60o were the values employed. At a p/e of 12, the Nu reached its greatest value, on the other side at a p/e = 8, f reached its highest value. The THP metric reached its greatest value with a p/e = 12 and an α = 60o.

In SAH shown in Figure 6, Aharwal, Gandhi and Saini [32] explored the impact of ribs by arranging inclined separated ribs in a rectangular channel. Consider the difference between the position ratio (d/w) and the relative gap width g/e. When compared to a plain channel, increases in Nu and f were 1.48 to 2.59 more than and 2.26 to 2.9 more than, respectively.

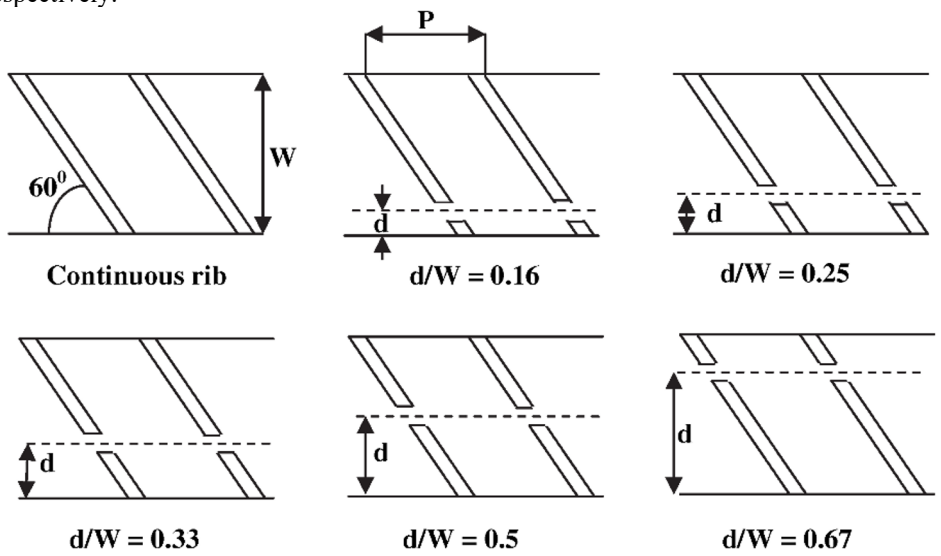

Figure 6 Transverse inclined ribs with gap [32]

Experimental studies on pressure drop, Δp, and heat transmission properties of an artificially roughened SAH channel with inclined wires were conducted by Gupta, Solanki and Saini [45]. They found that the f peaked at a 70° angle of attack, whereas the h peaked at a 60° angle.

2.4 Roughness element in expanded wire mesh fixation

By placing an extended metal mesh shape upon the absorber face of a SAH, as depicted in Figure 7, Saini and Saini and Saini [60] experimentally evaluated the impact on the h and f. The maximum Nu and f for fully generated zig-zag flow between rectangular channels along a high W/H = 11.1 were noticed to be 46.87, 71.87, and 25, 15 respectively. These values correspond to the relative L/e and S/e. The smooth absorber plate recorded the highest increase in Nu and f values of about 4 and 5 times, respectively.

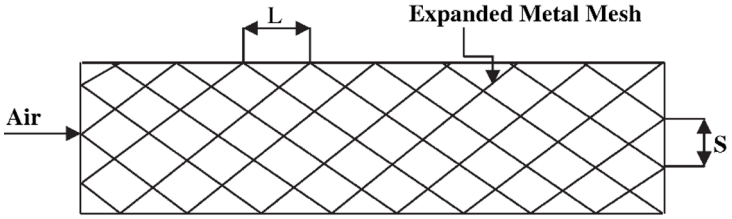

Figure 7 Expanded metal mesh [60]

2.5 Metal wire mesh roughness in discrete form

Further discrediting metal mesh, and grit ribs like those in Figure 8 were done by Karmare and Tikekar [30]. Re of 4000–17000, e/Dh of 0.034–0.043, p/e of 12.4–36, and l/s of 1.71–1 were among the parameter ranges. They demonstrated that plates with the roughness parameters l/s = 1.72 and p/e = 17.5 performed at their best.

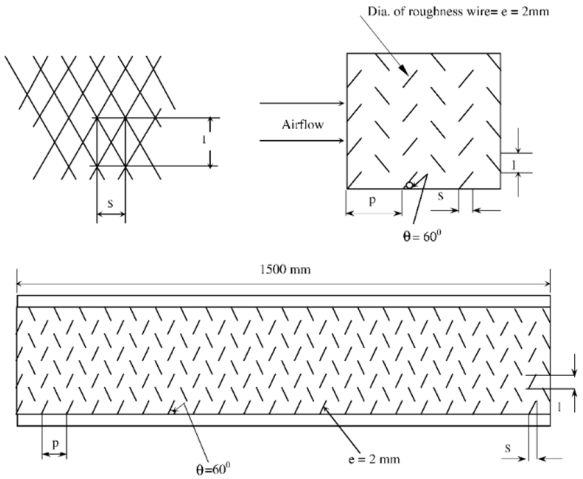

Figure 8 Metal grit ribs [30]

2.6 Chamfered roughness element

In an experiment, Karwa, Solanki and Saini [46] discovered the impact of roughness element in repeatedly separated chamfered upon absorber face, as shown in Figure 9. Along W/H of 4.7 to 12, p/e of 4.5 to 8.5, e/Dh of 0.0141 to 0.0328, and Re of 3000 to 20000. The roughness elements are chamfered at an angle between 15o and 18o. The 15o chamfered rib angles were determined to have the highest h and f. Due to the SAH chamfered rib roughened

absorber plate's increased Nu of between 50 and 120 percent, there was a noticeable increase in ηth of between 10 and 40 percent when compared to the smooth absorber plate.

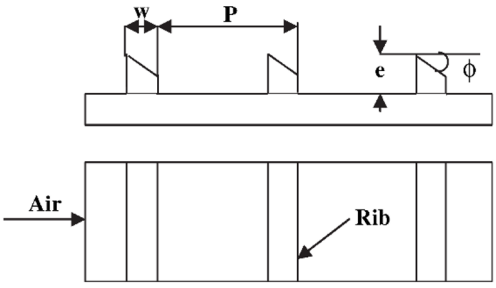

Figure 9 Integral chamfered ribs [46]

2.7 Wedge roughness element

In a SAH rectangular channel that was roughened with a wedge form transverse integral roughness element and shown in Figure 10, Bhagoria, Saini and Solanki [48] conducted an experimental investigation to determine influences for different parameters. Wedge angle (ϕ) ranged from 8 to 15o, p/e ranged from 60.17 to 12.12, e/Dh ranged from 0.015 to 0.033, and Re ranged from 3000 to 18000. It has been shown that a p/e of roughly 7.57 results in the most heat transmission. Pitch increased as relative roughness dropped and f increased. At a wedge angle of roughly 10o, heat transmission is enhanced most. According to the author, compared to a smooth duct, the Nu increased by 2.4 and 5.3 more, respectively.

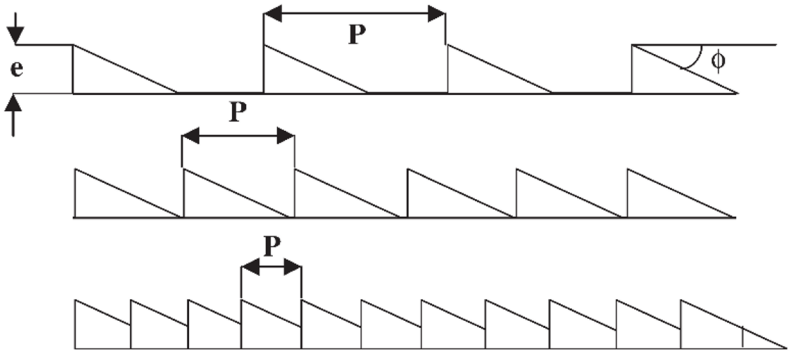

Figure 10 Wedge-Shaped Transverse Integral Ribs [48]

2.8 Regular W-ribs

Experimental research has been demonstrated by Lanjewar, Bhagoria and Sarviya [34] using the theory of a growing number of secondary cells in a w-shaped rib. The parameter's range was 0.018-0.03375 for e/Dh, 10 for p/e, and 30-75o for α. The highest enhancement of Nu along f was 2.36 along 2.01, respectively was found at α of 60o. Figure 11 roughness geometry is displayed.

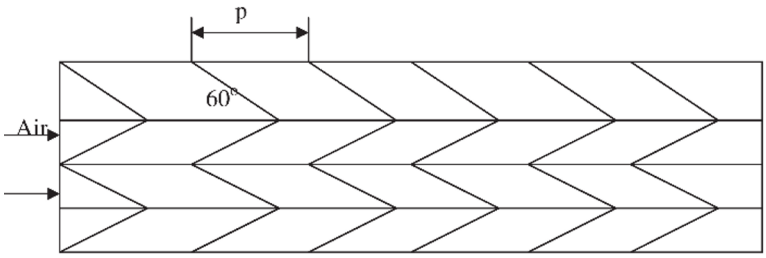

Figure 11 Continuous W ribs [34]

2.9 W roughness element in discrete form

In order to investigate the h expansion in a SAH with that absorber panel non-smooth along separated w from roughness, Kumar, Bhagoria and Sarviya [61] performed a laboratory investigation. e = 0.75 mm- 1 mm, e/Dh = 0.016- 0.0224, p/e = 10, Re = 3000- 15,000, and α of 45° were all included in the experiment. Beneath equal flow criterion, THP of non-smooth and smooth SAH were compared, and it was found that the roughened channel had THP that has been 1.2 to1.7 times greater for the range of criteria examined. Figure 12 illustrates the geometry that was examined.

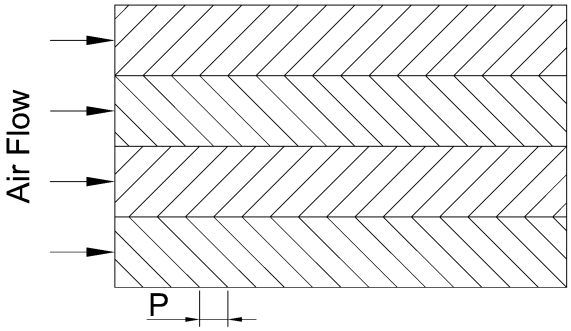

Figure 12 Discrete W ribs [61]

2.10 Combined roughness in a transverse and inclined manner

Using the notion of combined ribs in a transverse and inclined manner, Varun, Saini and Singal [33] explored. They discovered Re of 2000 to 14,000, e/Dh of 0.030, p/e of 3 to 8, and they also noted that roughened collectors with p values of 8 performed best.

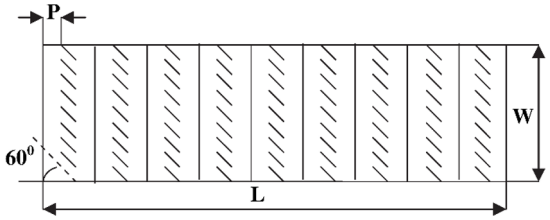

Figure 13 depicts the geometry of roughness.

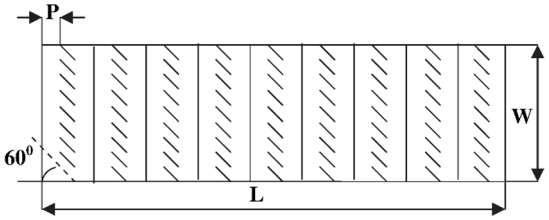

Figure 13 Transverse and inclined rib combination [33]

2.11 Combination of transverse with grove roughness element

Jaurker, Saini and Gandhi [49] investigated an experiment to see if transverse rib roughness could increase efficiency. p/e of 6 resulted in the greatest heat transmission. The g/p of 0.4 was discovered to provide the best heat transmission. Figure 14 depicts the geometry of roughness.

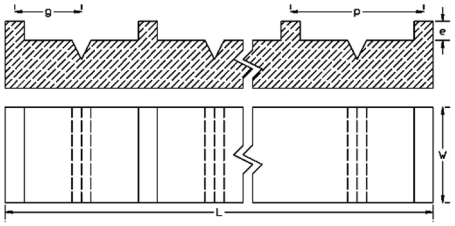

Figure 14 Transverse rib groove combinations [49]

2.12 Roughness element in combined form chamfered and grove manner

Layek, Saini and Solanki [50] studied the chamfered rib roughness. Re of 2000 to 21,000, e/Dh of 0.019 to 0.043, p/e of 4.5 to 10, α of 5 to 30o, and g/p of 0.3 to 0.6 were all included in the study. They discovered that the Nu along f enhanced through 3.23 and 0.77 respectively times, contrast to plain channel. When the g/p was 0.4, the Nu and f improved to their maximum levels. Figure 15 depicts the geometry of roughness.

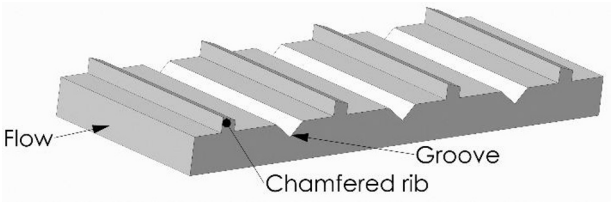

Figure 15 Chamfered rib groove combination [50]

2.13 Roughness element in an arc pattern

Saini and Saini [31] used an arc-shaped parallel wire shown in Figure 16, upon the absorber panel of a SAH to explore the influence of e/Dh and α/90 on h and f. With Re =2000–17000, e/Dh of 0.021–0.0422, and α/90 = 0.33–0.67 for a constant p/e = 10, the following specifications are used: The largest Nu enhancement was 3.80 times, which corresponds to an α/90 of 0.3333 at an e/Dh of 0.0422. However, it was discovered that the increase in f for these settings was just 1.75 times.

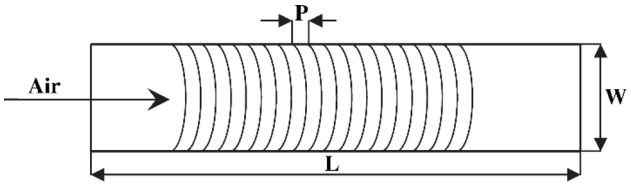

Figure 16.Arc-shaped ribs [31]

2.14 Roughness element in transverse dimple form

Saini and Verma [28] introduced the idea of roughness elements in the form of dimples. e/Dh = 0.018 - 0.037, p/e 8 - 12, and Re 2000 - 12,000. They discovered the highest e/Dh and p values to be 0.0379 and 10, respectively.

Figure 17 depicts the geometry of roughness. Using CFD, Yadav and Bhagoria [37] investigated Nu and f upon synthetically non-smooth SAH (CFD). Investigations have been done into how tiny circular transverse wire roughness influences Nu along f. The design factors considered are Re, p/e, and e/Dh). The ANSYS FLUENT 12.1 code is used to do a 2-D CFD simulation. THPP was used to estimate the requirements for optimum performance. For the range of parameters examined, a THPP with the highest range of 1.65 has been discovered.

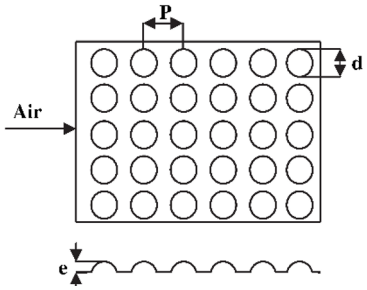

Figure 17 Transverse dimple roughness [28]

2.15 Roughness element in staggered dimple form

Bhushan and Singh [62], instead of transverse dimple roughness, the staggered dimple roughness element was examined. S/e = 18.75 - 37.50, L/e = 25.00 - 37.50, d/D = 0.147 - 0.36, e/Dh = 0.03-0.03, W/H ranged from 10 to 20, Re ranged from 4000 to 20,000. The maximum improvement upon Nu along f over a smooth duct under the given conditions was 3.8 and 2.2 times, respectively. S/e = 31.24, L/e = 31.24, and d/D = 0.294 were shown to have the greatest improvements in h. Figure 18 roughness geometry is displayed.

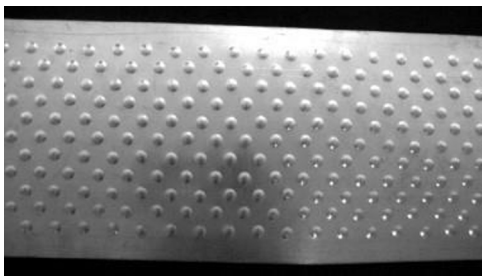

Figure 18 Staggered dimple roughness [62]

2.16 Roughness element in arc form 1

Yadav, Kaushal, Varun and Siddhartha [63] used dimple roughness with an arc form. Re = 3600 -18,000, p/e was between 12- 24, e/Dh was between 0.01- 0.03, and α of the protrusion configuration was between 45- 75o. For the parameter range under consideration, the maximum augmentation of the Nu along f has been noticed to be 2.89 along 2.93 more than, respectively, for a plain channel at e/Dh = 0.03, p/e = 12, along for an α = 60o. Figure 19 roughness geometry is displayed.

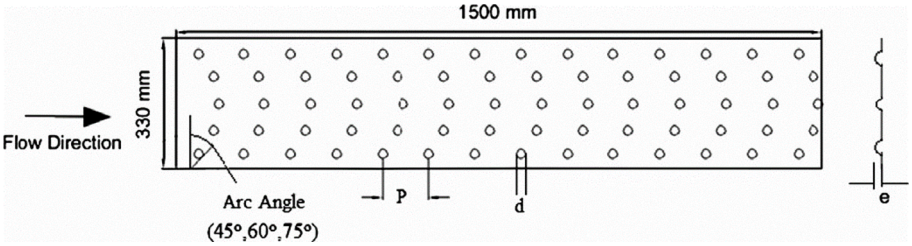

Figure 19 Roughness element in arc form [63]

2.17 Roughness element in arc form 2

Sethi, Varun and Thakur [52] used a different set of criteria when they looked into dimple-shaped roughness shown in Figure 20. The investigation encompassed the following parameters: e/Dh = 0.03, p/e = 12, and for α value of 60o. According to their report, the maximum Nu along an α = 60o, e/Dh = 0.036, and p/e =10.

Figure 20 Roughness element [52]

Singh, Varun and Siddhartha [39] considered Re values between 2200 and 22,000, e/Dh values between 0.018 and 0.045, α values between 30 and 75o, W/w =1-7, and p/e ranges between 4- 16 in the experimentally investigated. Correlations between the Nu and f were discovered by experimentation and gathered data, as illustrated in Figure 21.

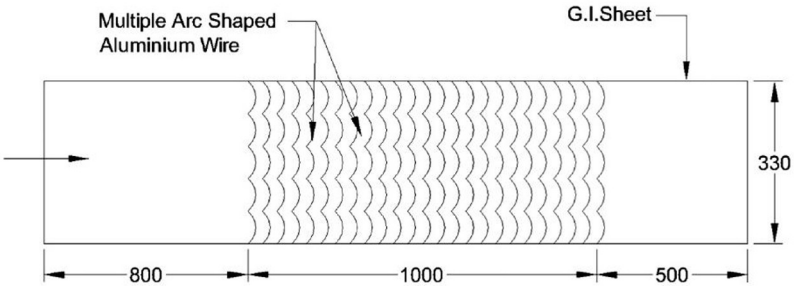

Figure 21 Multi arc Shaped [39]

Re 2100–21000, e/Dh of 0.016–0.044, p/e of 4–16, and α =30–75o, d/l = 0.25-0.85, W/w =1 to 7 were used in an experiment by Pandey, Bajpai and Varun [53]. Figure 22 illustrates the greatest improvement in Nu along f relative to the plain channel, which was 5.85 along 4.96 times, respectively.

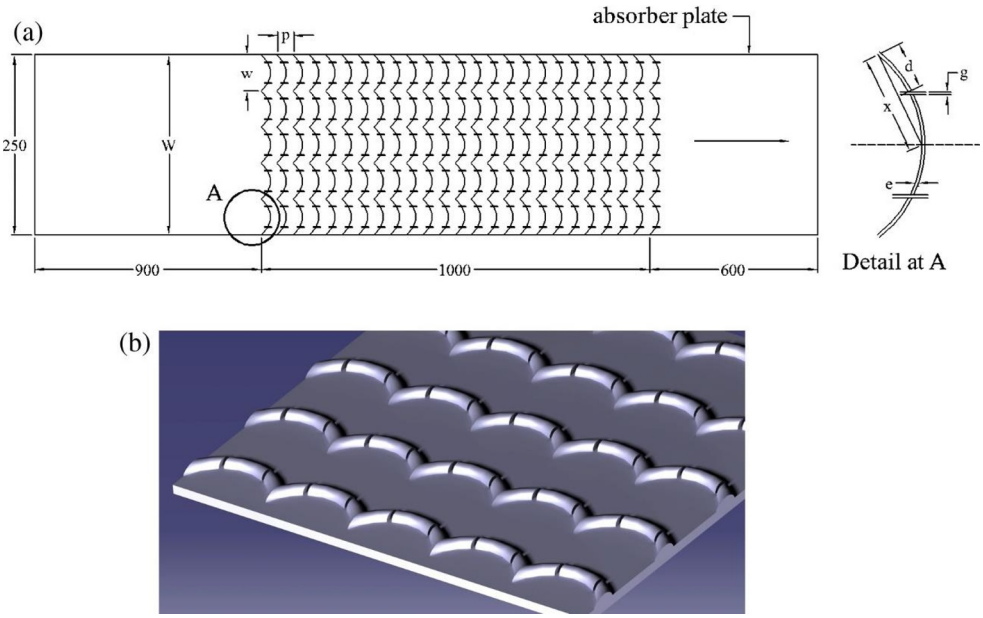

Figure 22.Multiple arcs with gap [53]

2.18 Roughness element in V -continuous form

Due to the rise in secondary vortices, Ebrahim Momin, Saini and Solanki [47] investigated inclined rib performed better than transverse ribs. There were more secondary vortices than before. They examined the roughness of the V-shaped ribs as depicted in Figure 23 and THP of the SAH for Re = 2500–18,000, e/Dh = 0.02 to 0.034, and α = 30 to 90o for

a constant p/e =10. For an arc angle of 60o degrees, the Nu along f were observed 2.30 along 2.83 more than that of a plain channel plate.

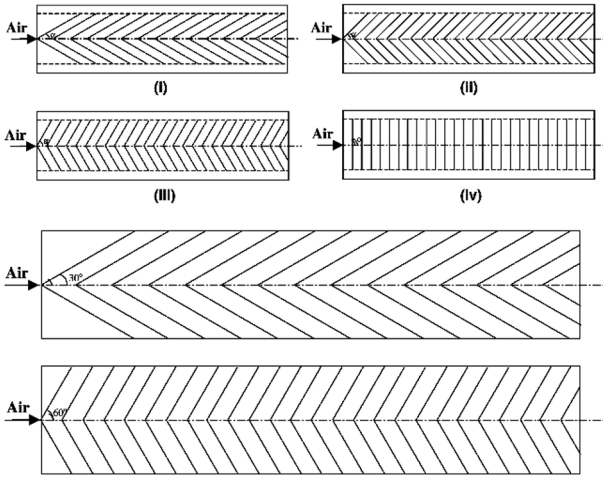

Figure 23 V shaped ribs continuous type [47]

2.19 Discrete type

Muluwork, Saini and Solanki [64] compared the THP of staggered separated v-apex up and v-down roughness element along equivalent separated roughness disproved the validity of V-shaped ribs. The researchers discovered that the Stanton number was greater for V-down discrete ribs than for the corresponding V-up and transverse discrete ribs. According to parameters research indicated in Figure 24, the St reported enhancement was 1.32-2.47.

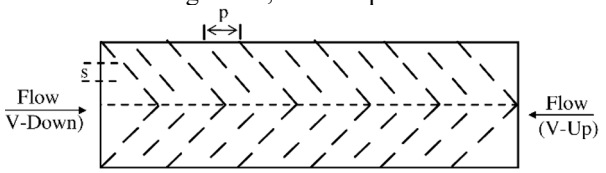

Figure 24 V-shaped discrete type [64]

A study by Karwa [15] used v-discontinuous and v-separated ribs. A= 45o–60o, and Re = 2850–15,500 were the parameter ranges (Figure 25). They discovered that discrete ribs outperform discontinuous ribs and that 60o ribs outperform 45o ribs.

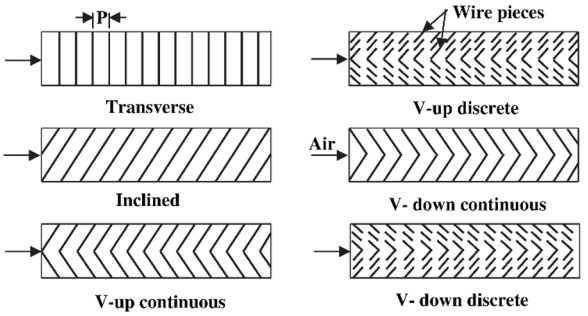

Figure 25 Applied ribs [15]

Separated v-down roughness (Figure 26) was examined by Singh, Chander and Saini [35]. Experiment has been run for Re = 3000 to 15,000 along g/e, d/w in 0.5 to 2.0 and 0.2 to 0.80 ranges, respectively. It also included e/Dh of 0.014–0.044, p/e of 4–12, and an α = 30–75o degrees. Maximum increases in Nusselt number along friction factor over a plain channel were 3.02 along 3.12 times, respectively, for roughness geometry. The rib parameters that increased with Nu along f were d/w = 0.65, g/e = 1.0, p/e = 10, α = 60o, and e/Dh = 0.043.

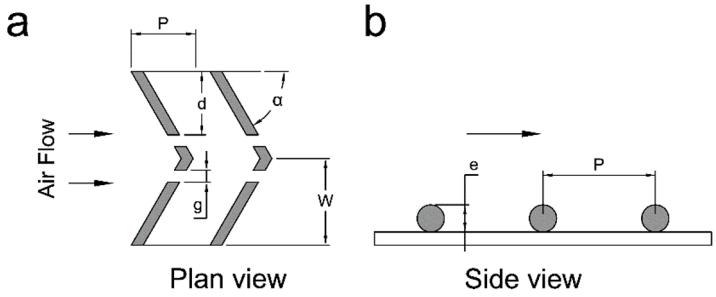

Figure 26 Applied ribs [35]

Multiple v-down roughness combined along staggered roughness was studied analytically and practically by Deo, Chander and Saini [41] for heat transfer and THP with Re =4000-12000, e/Dh=0.026 to 0.055, p/e = 4 to14, α = 40 to 80o, g/e of 1 (Figure 27). Nu and THP parameters both experienced maximal improvements of 3.34 and 2.45 times, respectively.

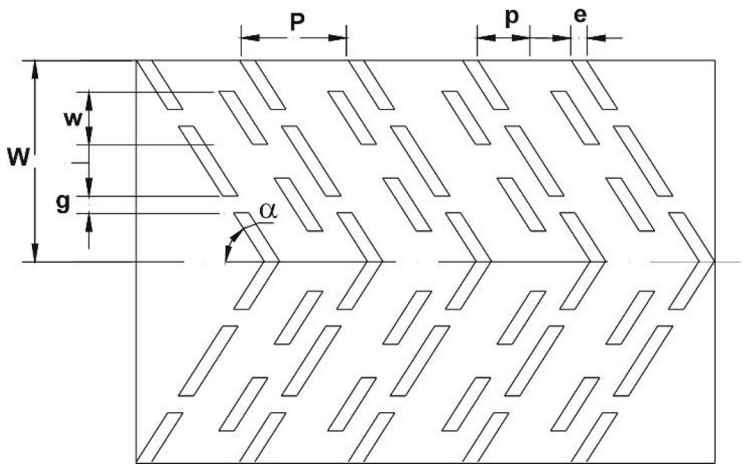

Figure 27 Discrete type roughness [41]

2.20 Roughness in multiple continuous forms

Using the theory of a rising number of secondary flow units, Hans, Saini and Saini [51] examined multiple continuous V- ribs. e/Dh of 0.019 to 0.043, p/e of 6 to 12, α of 30 to 75o, and W/w of 1 to 10, all of which were factors in the experiment. While f reached its maximum value for W/w of 10, the highest heat transmission occurred for W/w of 6. Both Nu along f

are 6.5 and 5.5 times higher than that eater plain duct of the parameter under investigation, respectively. Figure 28 depicts the geometry of roughness.

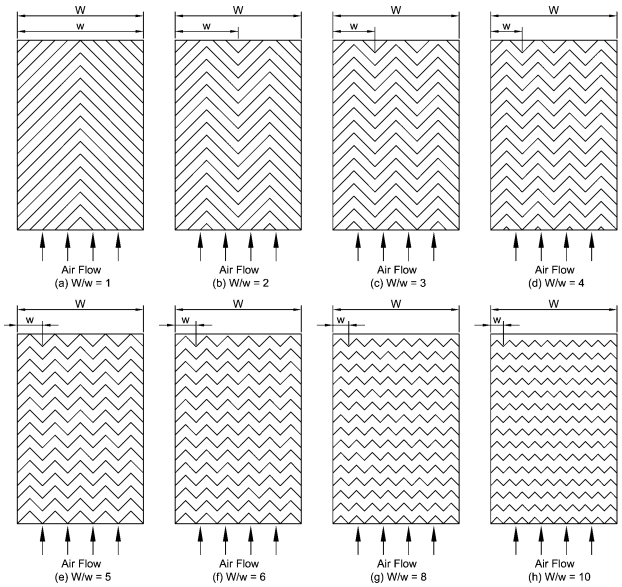

Figure 28.Multiple Continuous V Ribs [51]

2.21 Roughness in multiple forms with the gap

By creating a gap, Kumar, Saini and Saini [36] made use of the concepts of turbulence and flow acceleration. Re = 2000 - 20,000, relative width ratio was 6, Gd/Lv was 0.24 - 0.8, g/e was 0.5 to 1.5, and α was 60o. According to their findings, the highest improvement in Nu and f was 6.3 and 6.1more than that of a plain channel, respectively depicted in Figure 29.

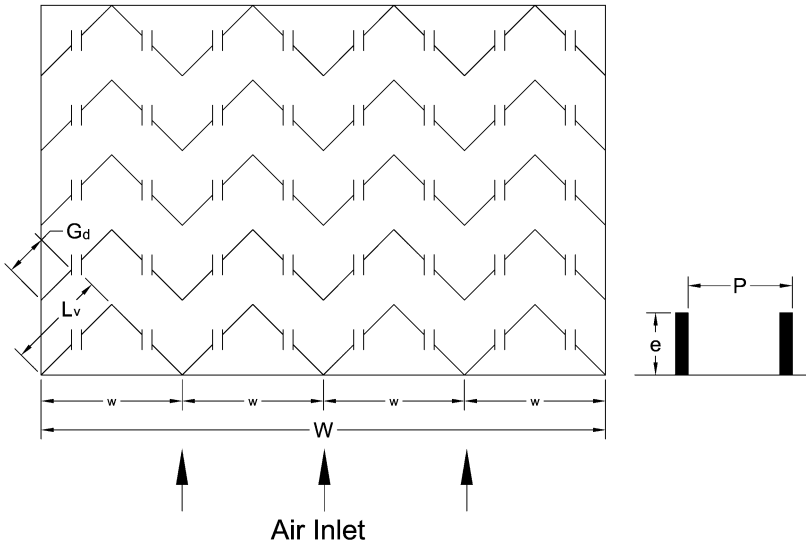

Figure 29.Multiple V-Ribs with Gap [36]

In a laboratory inspection by Maithani and Saini [42], v-ribs along uniform margins were employed as turbulence promoters to increase the h. e/Dh = 0.044, p/e = 6–12, α = 30–75o, g/e =1–5, and Ng = 1–5 were all factors that were examined. The f enhanced through 3.67 times higher than the plain duct, reaching a maximum enhancement of 3.6 more than that of the plain channel. According to Figure 30.

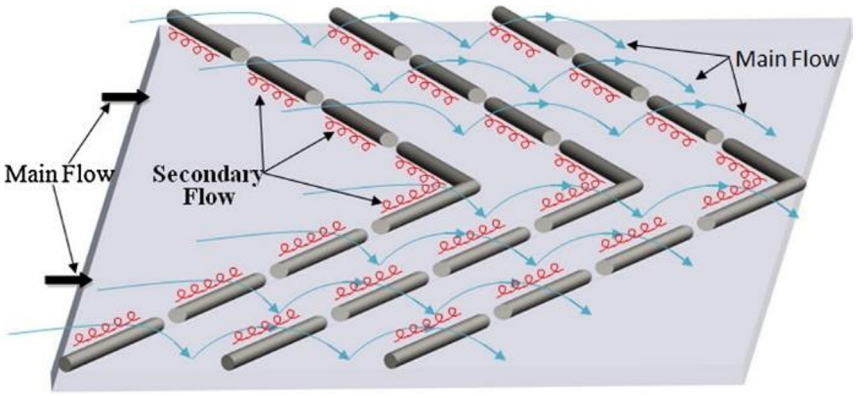

Figure 30.V Types Ribs with Symmetrical Gap [42]

With 60o angled cut manner more V baffles, Kumar, Kumar, Chauhan and Sethi [40] experimentally analysed of heat transfer enhancement included the following parameters: W/H =10; Re =3000-8000; WD/WB = 1-6; HB/HD = 0.5; PB/HB =10; Dd of 0.67; and relative gap width. From

Figure 31, the relative baffle width of five produced the highest overall thermal performance.

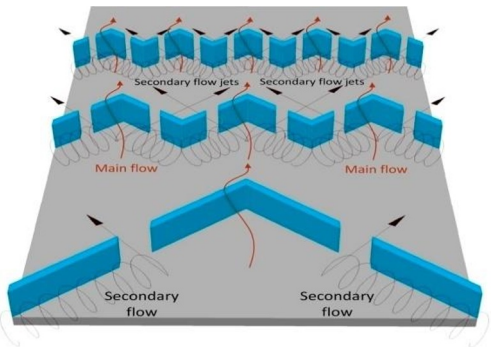

Figure 31 V Type Baffle [40]

Kumar, Prajapati and Samir [43] performed experimental analysis of Nu and f and their correlations development for SAH duct that was S roughness element with W/H of 12, p/e = 4-16, e/Dh = 0.021-0.053, W/w = 1-4, and Re of 2400-20000. According to experiment findings, the highest enhancement of Nusselt number along friction factor have been discovered at W/w of 3, p/e of 8, e/Dh of 0.043, and α of 60o, as depicted in Figure 32.

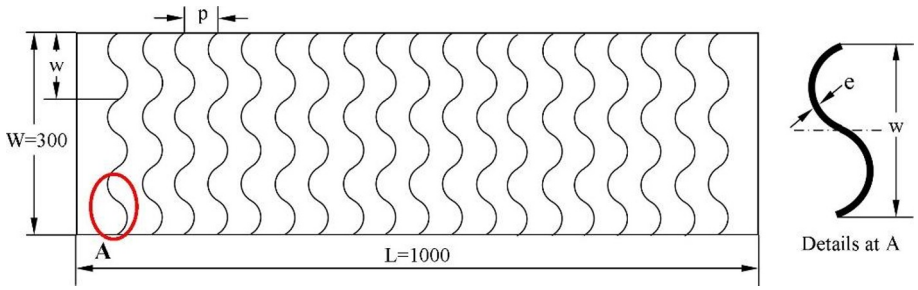

Figure 32 S Type Rib [43]

Sharma and Kalamkar [54] used computational and experimental techniques to evaluate the effects of different rib topologies on the functionality of this SAH. Along the span of pitch, two combined truncated and transverse roughness elements have been applied. The investigations were e/H of 0.1, e/Dh of 0.055, α of 90o, Re of 4000-16,000, and p/e of 10. The positioning of the ribs inside a roughened duct significantly influenced the performance of the SAH. Kumar, Kumar and Goel [65] discovered triangular duct section. The highest THPP, 2.75, is found in a rectangular roughness pattern with forwarding chamfering. Prakash and Saini [55] investigated different roughness in combined forms to determine how it affected the THP of a SAH. The laboratory parameters included 15 to 30 p/e, 2000 to 20,000 Re, 14 g/e, 0.04 e/Dh, and α = 60o. The maximum THPP range has been 3.66 at p/e = 25. In an experiment, performance of the SAH in respect to the effect of arc roughness in separated forms was examined by Kumar, Goel, Singh, Saxena, Kashyap and Rai [66]. The criterion of the study ranged from 0.3 to 0.9 in d/x, 1-3 in the number of gaps, and 0.5 to 1.5 in g/e. The THPP obtained its highest value of 3.85 by W/w of 1, d/x of 0.6, and Ng = 3. Using numerical and experimental techniques, Singh Patel and Lanjewar [56] examined the influences of innovative V form roughness upon the functionality of SAH. The range of the research parameter was p/e = 6 to 14, while other parameters, such as p'/p of 4, r/e of 4, g/e of 4, α of 60o, e/Dh of 0.043, and Ng of 3, had Re ranging from 4000 - 14,500. The highest improvement occurred in Nu of 1.55- 2.26 and f of 2.63 - 3.40 at p/e of 10 and 8, respectively, compared to a plain face. The maximum range of THPP of 1.59 has been reached at p/e of 10 and Re of 12,364. Correlations were also available for artificially roughened SAHs [39, 65, 67-73]. Alam, Kumar and Balam [57] quantitatively inspected the impact of protrusion roughness in the conical form on THP about SAH. The study's parameters were e/Dh of 0.02 - 0.044 and p/e of 6 – 12. Protrusions roughnesses in conical form have a significant influence on how well SAH works. Agrawal and Bhagoria [58] explained practical inspection upon influences of a particular kind of ribs without a gap on the THP of the SAH used a double-reverse arc pattern. The experimental parameters used were p/e = 8.33 and = 30°-75°, followed by p/e = 6.67 to 11.67 and α = 60°. The f was 0.0342 at e/Dh = 0.027, Re = 3010, and = 60°. Tanda and Satta [74] examined the effectiveness of a rectangular duct in relation to the effects of intersecting and 45° angled rib roughness. The flow was parallel to the ribs that connected them. The junction of the ribs boosted the duct's THP by increasing turbulence. Enhancement in Nusselt number (Nu) has been somewhat more when dual crossing roughness have been employed in place one of them crossing rib. The effects of a reverse roughness in double arc manner with uniform spacing upon SAH's performance were subject for experimental investigation by Agrawal, Bhagoria and Pagey [75]. Ranges of changed criterions were 10, 30, and 3000 to 14000 for p/e and Re, respectively. The smooth surface showed the biggest increases in friction factor and Nusselt number, which have been 2.4 and 2.8 much more than respectively. Maximum ranges of THPP, 2.41, has been found when p/e of 10 along e/Dh of 0.0270. In the course of their outdoor experimental operation, Agrawal, Bhagoria and Pagey [76], [77] discussed how to improve thermal efficiency for

discrete double arc reverse curved roughness elements. He discovered that the smooth plate had maximum values of h and ηth of 2.8 and 1.3, respectively. Additionally, experimental research has shown that Nu along f is 2.87 and 2.47 times stronger than on a smooth plate. Gawande, Dhoble, Zodpe and Fale [78] also used combined ribs. Table 3, lists the max value of Nu.

Table 3 Maximum enhancement in Nu found by investigators

Types of rib	Maximum enhancement in Nu
U-shaped [16]	2.82
W-shaped ribs [17]	2.16
Square [19]	2.89
Semi-circular [21]	2.34
Metal grit ribs [30]	1.87
Arc-shaped wire [31]	3.8
Discrete V-down ribs [35]	3.04
Circular [37]	2.31
Arc shaped [79]	1.7
Square [80]	2.73
Right-angle triangular [81]	3.1
equilateral triangular [82]	3.073
Chamfered square [83]	3.214
Square [84]	2.86
Saw-tooth [85]	1.78
Circular [86]	2.31
Rectangular tapered [87]	2.56
Circular [88]	2.53
Saw tooth [89]	2.18
Semi-circular [90]	2.76
Triangular [91]	2.7
Forward chamfered [92]	2.88
Semi-circular [93]	3.24
Circular [94]	2.47
Triangular [95]	2.94
Semi-circular [96]	2.08
Square wave [97]	2.14
Equilateral triangular [98]	2.82
450 protrude and dimpled rib [99]	4.67
Clerestory [100]	1.82
Circular and semi-circular [101]	3.05
Gap arc geometry and staggered element [102]	2.18
Winglet shaped ribs [103]	2.83

3. Conclusion

This research attempts to present the h and f characteristics of a SAH artificially roughened duct utilizing various rib geometries. The given conclusion is reached in light of the literature review:

1. Roughness elements used in SAH are a useful way to enhance heat movement to fluid moving across channel and it reported maximum transfer of heat compared to the plain surface under the uniform variable criterion. It has been determined that the various

roughness geometry types employed in SAH depend on the configurations and positions of the ribs upon the absorber panel.

2. When the surface of a SAH is roughened, the-rest noticeable enhancement in h along with an increase in flow friction. However, for each sort of rib geometry used, several researchers find a different number of increments in Nusselt number and friction factor.
3. There are many different types of parameters that identify roughness elements, but the repetitive roughness element geometry for SAH is best defined by the dimensionless parameter. Specifically, aspect ratio (W/H), relative roughness pitch (p/e), relative roughness height (e/Dh), and angle of arc (α). Less W/H ranges provide higher THP in SAH along ducting whereas high W/H values have better ηth.
4. Different industries use SAH in different ways. A certain form of geometry can be chosen depending on the energy needed. In this regard, the reviews in this paper may be helpful. By using artificial roughness, it can be recognized that more friction factor (f) results in higher pumping power needs. It is ideal for the SAH to be designed to transfer the most heat energy to the moving fluid while using the least amount of blower energy possible.
5. The numerous correlations created for Nusselt number and friction factor depends on the system operating parameters and researchers in their efforts to determine the values of the options.
6. For the analyzed range of parameters, it was discovered that the usage of arc-shaped-shaped rib geometry and metal grit ribs has the maximum THP parameters in comparison to often roughness geometry. For the tested range of parameters, the use of broken arc ribs has the highest Nu compared to the plain arc-shaped rib roughness.
7. The use of a V-type baffle presented a well-known highest total THP that appeared at an analogous baffle thickness compared to arc-shaped with different configurations and v-type discrete shaped.
8. The THP over the continuous ribs has significantly improved since gaps were made in them. The increase in pumping force is required because of the improvement in Nusselt number (Nu) caused by the gaps formed upon the gap from roughness elements against 1.0 to 1.4 assets.
9. The highest THPP values are observed for an S pattern roughness, several V patterns, and arc pattern roughness in separated forms.
10. Arc configuration of roughness element exhibits fewer ranges pressure diminishes than the V form design because the produced secondary flow has a curved structure and is rougher.

Finally, this article discusses the concept of artificial roughness used in the design of SAHs. It will provide useful information for researchers to carry out the necessary studies to find out the optimal design of the system. This article, according to the authors, will have given researchers a better understanding of artificial roughness.

References

1. Sukhatme S P and Nayak J K 2017 Solar energy (India: McGraw-Hill Education)
2. Karwa R and Srivastava V 2013 Thermal Performance of Solar Air Heater Having Absorber Plate with V-Down Discrete Rib Roughness for Space-Heating Applications Journal of Renewable Energy 2013 151578
3. Shamsul Azha N I, Hussin H, Nasif M S and Hussain T 2020 Thermal Performance Enhancement in Flat Plate Solar Collector Solar Water Heater: A Review Processes 8

4. Yadav A S and Thapak M K 2016 Artificially roughened solar air heater: A comparative study International Journal of Green Energy 13 143-72
5. Yadav A S and Thapak M K 2014 Artificially roughened solar air heater: Experimental investigations Renewable and Sustainable Energy Reviews 36 370-411
6. Sharma S K and Kalamkar V R 2016 Computational Fluid Dynamics approach in thermo-hydraulic analysis of flow in ducts with rib roughened walls – A review Renewable and Sustainable Energy Reviews 55 756-88
7. Yadav A S, Gupta S, Agrawal A, Saxena R, Agrawal N and Nashine S 2022 Performance enhancement of solar air heater by attaching artificial rib roughness on the absorber Plate Materials Today: Proceedings 63 706-17
8. Gawande V B, Dhoble A S, Zodpe D B and Chamoli S 2016 A review of CFD methodology used in literature for predicting thermo-hydraulic performance of a roughened solar air heater Renewable and Sustainable Energy Reviews 54 550-605
9. Yadav A S, Prakash Shukla O and Singh Bhadoria R 2022 Recent advances in modeling and simulation techniques used in analysis of solar air heater having ribs Materials Today: Proceedings 62 1375-82
10. Yadav A S, Agrawal A, Sharma A and Gupta A 2022 Revisiting the effect of ribs on performance of solar air heater using CFD approach Materials Today: Proceedings 63 240-52
11. Tyagi V V, Panwar N L, Rahim N A and Kothari R 2012 Review on solar air heating system with and without thermal energy storage system Renewable and Sustainable Energy Reviews 16 2289-303
12. Balaras C A 1990 A review of augmentation techniques for heat transfer surfaces in single-phase heat exchangers Energy 15 899-906
13. Lau S C, McMillin R D and Han J C 1991 Turbulent Heat Transfer and Friction in a Square Channel With Discrete Rib Turbulators Journal of Turbomachinery 113 360-6
14. Zhang Y M, Gu W Z and Han J C 1994 Heat Transfer and Friction in Rectangular Channels With Ribbed or Ribbed-Grooved Walls Journal of Heat Transfer 116 58-65
15. Karwa R 2003 Experimental studies of augmented heat transfer and friction in asymmetrically heated rectangular ducts with ribs on the heated wall in transverse, inclined, v-continuous and v-discrete pattern International Communications in Heat and Mass Transfer 30 241-50
16. Bopche S B and Tandale M S 2009 Experimental investigations on heat transfer and frictional characteristics of a turbulator roughened solar air heater duct International Journal of Heat and Mass Transfer 52 2834-48
17. Kumar A, Bhagoria J L and Sarviya R M 2009 Heat transfer and friction correlations for artificially roughened solar air heater duct with discrete W-shaped ribs Energy Conversion and Management 50 2106-17
18. Lanjewar A, Bhagoria J L and Sarviya R M 2011 Heat transfer and friction in solar air heater duct with W-shaped rib roughness on absorber plate Energy 36 4531-41
19. Yadav A S and Bhagoria J L 2013 Modeling and Simulation of Turbulent Flows through a Solar Air Heater Having Square-Sectioned Transverse Rib Roughness on the Absorber Plate The Scientific World Journal 2013 827131

20. Yadav A S and Bhagoria J L 2013 Heat transfer and fluid flow analysis of solar air heater: A review of CFD approach Renewable and Sustainable Energy Reviews 23 60-79
21. Yadav A S and Bhagoria J L 2014 A Numerical Investigation of Turbulent Flows through an Artificially Roughened Solar Air Heater Numerical Heat Transfer, Part A: Applications 65 679-98
22. Lanjewar A M, Bhagoria J L and Agrawal M K 2015 Review of development of artificial roughness in solar air heater and performance evaluation of different orientations for double arc rib roughness Renewable and Sustainable Energy Reviews 43 1214-23
23. Gawande V B, Dhoble A S, Zodpe D B and Chamoli S 2016 Analytical approach for evaluation of thermo hydraulic performance of roughened solar air heater Case Studies in Thermal Engineering 8 19-31
24. Gawande V B, Dhoble A S, Zodpe D B and Chamoli S 2016 Experimental and CFD investigation of convection heat transfer in solar air heater with reverse L-shaped ribs Solar Energy 131 275-95
25. Joule J P 1861 VIII. On the surface-condensation of steam Philosophical transactions of the Royal Society of London 133-60
26. Prasad K and Mullick S C 1983 Heat transfer characteristics of a solar air heater used for drying purposes Applied Energy 13 83-93
27. Prasad B N 2013 Thermal performance of artificially roughened solar air heaters Solar Energy 91 59-67
28. Saini R P and Verma J 2008 Heat transfer and friction factor correlations for a duct having dimple-shape artificial roughness for solar air heaters Energy 33 1277-87
29. Sahu M M and Bhagoria J L 2005 Augmentation of heat transfer coefficient by using 90° broken transverse ribs on absorber plate of solar air heater Renewable Energy 30 2057-73
30. Karmare S V and Tikekar A N 2007 Heat transfer and friction factor correlation for artificially roughened duct with metal grit ribs International Journal of Heat and Mass Transfer 50 4342-51
31. Saini S K and Saini R P 2008 Development of correlations for Nusselt number and friction factor for solar air heater with roughened duct having arc-shaped wire as artificial roughness Solar Energy 82 1118-30
32. Aharwal K R, Gandhi B K and Saini J S 2008 Experimental investigation on heat-transfer enhancement due to a gap in an inclined continuous rib arrangement in a rectangular duct of solar air heater Renewable Energy 33 585-96
33. Varun, Saini R P and Singal S K 2008 Investigation of thermal performance of solar air heater having roughness elements as a combination of inclined and transverse ribs on the absorber plate Renewable Energy 33 1398-405
34. Lanjewar A, Bhagoria J L and Sarviya R M 2011 Experimental study of augmented heat transfer and friction in solar air heater with different orientations of W-Rib roughness Experimental Thermal and Fluid Science 35 986-95
35. Singh S, Chander S and Saini J S 2011 Heat transfer and friction factor correlations of solar air heater ducts artificially roughened with discrete V-down ribs Energy 36 5053-64

36. Kumar A, Saini R P and Saini J S 2012 Experimental investigation on heat transfer and fluid flow characteristics of air flow in a rectangular duct with Multi v-shaped rib with gap roughness on the heated plate Solar Energy 86 1733-49
37. Yadav A S and Bhagoria J L 2013 A CFD (computational fluid dynamics) based heat transfer and fluid flow analysis of a solar air heater provided with circular transverse wire rib roughness on the absorber plate Energy 55 1127-42
38. Bharadwaj G, Kaushal M and Goel V 2013 Heat transfer and friction characteristics of an equilateral triangular solar air heater duct using inclined continuous ribs as roughness element on the absorber plate International Journal of Sustainable Energy 32 515-30
39. Singh A P, Varun and Siddhartha 2014 Heat transfer and friction factor correlations for multiple arc shape roughness elements on the absorber plate used in solar air heaters Experimental Thermal and Fluid Science 54 117-26
40. Kumar R, Kumar A, Chauhan R and Sethi M 2016 Heat transfer enhancement in solar air channel with broken multiple V-type baffle Case Studies in Thermal Engineering 8 187-97
41. Deo N S, Chander S and Saini J S 2016 Performance analysis of solar air heater duct roughened with multigap V-down ribs combined with staggered ribs Renewable Energy 91 484-500
42. Maithani R and Saini J S 2016 Heat transfer and friction factor correlations for a solar air heater duct roughened artificially with V-ribs with symmetrical gaps Experimental Thermal and Fluid Science 70 220-7
43. Kumar K, Prajapati D R and Samir S 2017 Heat transfer and friction factor correlations development for solar air heater duct artificially roughened with ‘S’ shape ribs Experimental Thermal and Fluid Science 82 249-61
44. Prasad B N and Saini J S 1988 Effect of artificial roughness on heat transfer and friction factor in a solar air heater Solar Energy 41 555-60
45. Gupta D, Solanki S C and Saini J S 1997 Thermohydraulic performance of solar air heaters with roughened absorber plates Solar Energy 61 33-42
46. Karwa R, Solanki S C and Saini J S 2001 Thermo-hydraulic performance of solar air heaters having integral chamfered rib roughness on absorber plates Energy 26 161-76
47. Ebrahim Momin A-M, Saini J S and Solanki S C 2002 Heat transfer and friction in solar air heater duct with V-shaped rib roughness on absorber plate International Journal of Heat and Mass Transfer 45 3383-96
48. Bhagoria J L, Saini J S and Solanki S C 2002 Heat transfer coefficient and friction factor correlations for rectangular solar air heater duct having transverse wedge shaped rib roughness on the absorber plate Renewable Energy 25 341-69
49. Jaurker A R, Saini J S and Gandhi B K 2006 Heat transfer and friction characteristics of rectangular solar air heater duct using rib-grooved artificial roughness Solar Energy 80 895-907
50. Layek A, Saini J S and Solanki S C 2007 Second law optimization of a solar air heater having chamfered rib–groove roughness on absorber plate Renewable Energy 32 1967-80
51. Hans V S, Saini R P and Saini J S 2010 Heat transfer and friction factor correlations for a solar air heater duct roughened artificially with multiple v-ribs Solar Energy 84 898-911

52. Sethi M, Varun and Thakur N S 2012 Correlations for solar air heater duct with dimpled shape roughness elements on absorber plate Solar Energy 86 2852-61
53. Pandey N K, Bajpai V K and Varun 2016 Experimental investigation of heat transfer augmentation using multiple arcs with gap on absorber plate of solar air heater Solar Energy 134 314-26
54. Sharma S K and Kalamkar V R 2017 Experimental and numerical investigation of forced convective heat transfer in solar air heater with thin ribs Solar Energy 147 277-91
55. Prakash C and Saini R P 2019 Heat transfer and friction in rectangular solar air heater duct having spherical and inclined rib protrusions as roughness on absorber plate Experimental Heat Transfer 32 469-87
56. Singh Patel S and Lanjewar A 2019 Experimental and numerical investigation of solar air heater with novel V-rib geometry Journal of Energy Storage 21 750-64
57. Alam T, Kumar A and Balam N B 2020 Thermo-Hydraulic Performance of Solar Air Heater Duct Provided with Conical Protrusion Rib Roughnesses. In: Advances in Energy Research, Vol. 2, ed S Singh and V Ramadesigan (Singapore: Springer Singapore) pp 159-68
58. Agrawal Y and Bhagoria J L 2021 Experimental investigation for pitch and angle of arc effect of discrete artificial roughness on Nusselt number and fluid flow characteristics of a solar air heater Materials Today: Proceedings 46 5506-11
59. Kumar S T, Mittal V, Thakur N S and Kumar A 2011 Heat transfer and friction factor correlations for rectangular solar air heater duct having 60 inclined continuous discrete rib arrangement Br J Appl Sci Technol 3 67-93
60. Saini R P and Saini J S 1997 Heat transfer and friction factor correlations for artificially roughened ducts with expanded metal mesh as roughness element International Journal of Heat and Mass Transfer 40 973-86
61. Kumar A, Bhagoria J L and Sarviya R M Heat transfer enhancement in channel of solar air collector by using discrete w-shaped artificial roughened absorber.
62. Bhushan B and Singh R 2011 Nusselt number and friction factor correlations for solar air heater duct having artificially roughened absorber plate Solar Energy 85 1109-18
63. Yadav S, Kaushal M, Varun and Siddhartha 2013 Nusselt number and friction factor correlations for solar air heater duct having protrusions as roughness elements on absorber plate Experimental Thermal and Fluid Science 44 34-41
64. Muluwork K B, Saini J S and Solanki S C 1998 Studies on discrete rib roughened solar air heaters. p 84
65. Kumar R, Kumar A and Goel V 2019 Performance improvement and development of correlation for friction factor and heat transfer using computational fluid dynamics for ribbed triangular duct solar air heater Renewable Energy 131 788-99
66. Kumar R, Goel V, Singh P, Saxena A, Kashyap A S and Rai A 2019 Performance evaluation and optimization of solar assisted air heater with discrete multiple arc shaped ribs Journal of Energy Storage 26 100978
67. Maithani R, Chamoli S, Kumar A and Gupta A 2019 Solar air heater duct roughened with wavy delta winglets: correlations development and parametric optimization Heat and Mass Transfer

68. Yadav A S, Shrivastava V, Ravi Kiran T and Dwivedi M K 2021 Recent Advances in Mechanical Engineering, Lecture Notes in Mechanical Engineering, ed A Kumar, et al. (Singapore: Springer) pp 217-26
69. Yadav A S, Shrivastava V, Sharma A and Dwivedi M K 2021 Numerical simulation and CFD-based correlations for artificially roughened solar air heater Materials Today: Proceedings 47 2685-93
70. Kumar V 2019 Nusselt number and friction factor correlations of three sides concave dimple roughened solar air heater Renewable Energy 135 355-77
71. Yadav A S, Dwivedi M K, Sharma A and Chouksey V K 2022 CFD based heat transfer correlation for ribbed solar air heater Materials Today: Proceedings 62 1402-7
72. Kumar R, Chauhan R, Sethi M and Kumar A 2017 Experimental study and correlation development for Nusselt number and friction factor for discretized broken V-pattern baffle solar air channel Experimental Thermal and Fluid Science 81 56-75
73. Kumar A and Layek A 2019 Nusselt number and friction factor correlation of solar air heater having twisted-rib roughness on absorber plate Renewable Energy 130 687-99
74. Tanda G and Satta F 2021 Heat transfer and friction in a high aspect ratio rectangular channel with angled and intersecting ribs International Journal of Heat and Mass Transfer 169 120906
75. Agrawal Y, Bhagoria J L and Pagey V S 2021 Enhancement of thermo-hydraulic performance using double arc reverse ribs in a solar collector: Experimental approach Materials Today: Proceedings 47 6067-73
76. Agrawal Y, Bhagoria J L and Pagey V S 2022 Enhancement of thermal efficiency of solar air collector by using discrete double arc reverse shaped roughness on the absorber plate Materials Today: Proceedings 51 1548-53
77. Agrawal Y, Bhagoria J L, Gautam A, Kumar Chaurasiya P, Arockia Dhanraj J, Muthiya Solomon J and Salyan S 2022 Experimental evaluation of hydrothermal performance of solar air heater with discrete roughened plate Applied Thermal Engineering 211 118379
78. Gawande V B, Dhoble A S, Zodpe D B and Fale S G 2020 Thermal performance evaluation of solar air heater using combined square and equilateral triangular rib roughness Australian Journal of Mechanical Engineering 18 234-44
79. Kumar S and Saini R P 2009 CFD based performance analysis of a solar air heater duct provided with artificial roughness Renewable Energy 34 1285-91
80. Yadav A S and Bhagoria J L 2015 Numerical investigation of flow through an artificially roughened solar air heater International Journal of Ambient Energy 36 87-100
81. Gawande V B, Dhoble A S, Zodpe D B and Chamoli S 2015 Experimental and CFD-based thermal performance prediction of solar air heater provided with right-angle triangular rib as artificial roughness Journal of the Brazilian Society of Mechanical Sciences and Engineering 38 551-79
82. Yadav A S and Bhagoria J L 2014 A CFD based thermo-hydraulic performance analysis of an artificially roughened solar air heater having equilateral triangular sectioned rib roughness on the absorber plate International Journal of Heat and Mass Transfer 70 1016-39

83. Gawande V B, Dhoble A S, Zodpe D B and Chamoli S 2015 Experimental and CFD-based thermal performance prediction of solar air heater provided with chamfered square rib as artificial roughness Journal of the Brazilian Society of Mechanical Sciences and Engineering 38 643-63
84. Yadav A S and Bhagoria J L 2014 A numerical investigation of square sectioned transverse rib roughened solar air heater International Journal of Thermal Sciences 79 111-31
85. Singh S, Singh B, Hans V S and Gill R S 2015 CFD (computational fluid dynamics) investigation on Nusselt number and friction factor of solar air heater duct roughened with non-uniform cross-section transverse rib Energy 84 509-17
86. Yadav A S and Bhagoria J L 2014 Heat transfer and fluid flow analysis of an artificially roughened solar air heater: a CFD based investigation Frontiers in Energy 8 201-11
87. Gupta A D and Varshney L 2017 Performance prediction for solar air heater having rectangular sectioned tapered rib roughness using CFD Thermal Science and Engineering Progress 4 122-32
88. Yadav A S 2015 CFD investigation of effect of relative roughness height on Nusselt number and friction factor in an artificially roughened solar air heater Journal of the Chinese Institute of Engineers 38 494-502
89. Singh A and Singh S 2017 CFD investigation on roughness pitch variation in non-uniform cross-section transverse rib roughness on Nusselt number and friction factor characteristics of solar air heater duct Energy 128 109-27
90. Yadav A S, Alam T, Gupta G, Saxena R, Gupta N K, Allamraju K V, Kumar R, Sharma N, Sharma A, Pandey U and Agrawal Y 2022 A Numerical Investigation of an Artificially Roughened Solar Air Heater Energies 15 8045
91. Yadav A S and Bhagoria J L 2013 A CFD analysis of a solar air heater having triangular rib roughness on the absorber plate International Journal of ChemTech Research 5 964-71
92. Kumar R, Goel V and Kumar A 2018 Investigation of heat transfer augmentation and friction factor in triangular duct solar air heater due to forward facing chamfered rectangular ribs: A CFD based analysis Renewable Energy 115 824-35
93. Yadav A S, Mishra A, Dwivedi K, Agrawal A, Galphat A and Sharma N 2022 Investigation on performance enhancement due to rib roughened solar air heater Materials Today: Proceedings 63 726-30
94. Kumar R, Goel V, Kumar A, Khurana S, Singh P and Bopche S B 2018 Numerical investigation of heat transfer and friction factor in ribbed triangular duct solar air heater using Computational fluid dynamics (CFD) Journal of Mechanical Science and Technology 32 399-404
95. Prasad R, Yadav A S, Singh N K and Johari D 2019 Advances in Fluid and Thermal Engineering, Lecture Notes in Mechanical Engineering, ed P Saha, et al. (Singapore: Springer) pp 613-26
96. Yadav A S, Shrivastava V, Chouksey V K, Sharma A, Sharma S K and Dwivedi M K 2021 Enhanced solar thermal air heater: A numerical investigation Materials Today: Proceedings 47 2777-83
97. Singh I and Singh S 2018 CFD analysis of solar air heater duct having square wave profiled transverse ribs as roughness elements Solar Energy 162 442-53

98. Yadav A S and Sharma S K 2021 Advances in Fluid and Thermal Engineering, Lecture Notes in Mechanical Engineering, ed B S Sikarwar, et al. (Singapore: Springer) pp 549-58
99. Kumar A, Maithani R, Yadav A S and Sharma S 2022 Effect of 450 protruded and dimpled rib height on the performance of triangular duct solar heat collector Materials Today: Proceedings 63 253-8
100. Fernandes D V and Manjunath M S 2021 A CFD analysis on the influence of upstream surface geometry modifications of clerestory shaped rib on heat transfer characteristics of solar air heater International Journal of Automotive and Mechanical Engineering 18 8907-26
101. Yadav A S, Shukla O P, Sharma A and Khan I A 2022 CFD analysis of heat transfer performance of ribbed solar air heater Materials Today: Proceedings 62 1413-9
102. Ambade J and Lanjewar A 2019 Experimental investigation of solar air heater with new symmetrical gap arc geometry and staggered element International Journal of Thermal Sciences 146 106093
103. Kumar A and Layek A 2022 Evaluation of the performance analysis of an improved solar air heater with Winglet shaped ribs Experimental Heat Transfer 35 239-57